Draft version September 9, 2013
Preprint typeset using LaTeX style emulateapj v. 5/2/11

ON DISCOVERING ELECTROMAGNETIC EMISSION FROM NEUTRON STAR MERGERS: THE EARLY YEARS OF TWO GRAVITATIONAL WAVE DETECTORS

Mansi M. Kasliwal[1] & Samaya Nissanke[2]

Draft version September 9, 2013

ABSTRACT

We present the first simulation addressing the prospects of finding an electromagnetic (EM) counterpart to gravitational wave detections (GW) during the early years of only two advanced interferometers. The perils of such a search may have appeared insurmountable when considering the coarse ring-shaped GW localizations spanning thousands of deg^2 using time-of-arrival information alone. We show that leveraging the amplitude and phase information of the predicted GW signal narrows the localization to arcs with a median area of only ≈ 250 deg^2, thereby making an EM search tractable. Based on the locations and orientations of the two LIGO detectors, we find that the GW sensitivity is limited to one polarization and thus to only two sky quadrants. Thus, the rates of GW events with two interferometers is only $\approx$40% of the rate with three interferometers of similar sensitivity. Another important implication of the sky quadrant bias is that EM observatories in North America and Southern Africa would be able to systematically respond to GW triggers several hours sooner than Russia and Chile. Given the larger sky areas and the relative proximity of detected mergers, 1m-class telescopes with very wide-field cameras are well positioned for the challenge of finding an EM counterpart. Identification of the EM counterpart amidst the even larger numbers of false positives further underscores the importance of building a comprehensive catalog of foreground stellar sources, background AGN and potential host galaxies in the local universe.

Subject headings: gravitational waves — binaries: close — stars: neutron — surveys — catalogs

1. INTRODUCTION

The advent of advanced ground-based interferometers this decade is expected to usher in the era of *routine* gravitational wave (GW) detection (Barish & Weiss 1999; LIGO Scientific Collaboration 2008; Accadia et al. 2011; Somiya 2012). Binary neutron star (NS) mergers are anticipated to be amongst the most numerous and strongest GW sources (Abadie et al. 2010). NS mergers are predicted to produce neutron-rich outflows and emit electromagnetic (EM) radiation across many wavelengths and timescales as the ejected debris interacts with its environment — gamma (e.g., Eichler et al. 1989; Paczynski 1991; Narayan et al. 1992), optical (e.g., Li & Paczyński 1998; Kulkarni 2005; Metzger et al. 2010; Roberts et al. 2011; Piran et al. 2012; Rosswog 2013), infrared (e.g., Barnes & Kasen 2013; Kasen et al. 2013; Tanaka & Hotokezaka 2013; Grossman et al. 2013) and radio (e.g., Hansen & Lyutikov 2001; Pshirkov & Postnov 2010; Nakar & Piran 2011).

The discovery and characterization of the EM counterparts to GW detections promises to unravel astrophysics in the strong field gravity regime. Moreover, such EM-GW events will serve as the litmus test for whether NS mergers are indeed the sites of r-process nucleosynthesis (and hence, responsible for producing half the elements heavier than iron including gold, platinum and uranium; e.g. Lattimer & Schramm 1976; Mathews & Cowan 1990). The accompanying surge of excitement in preparation for this endeavor has been described as analogous to the "gold rush" (Kasliwal 2013).

[1] The Observatories, Carnegie Institution for Science, 813 Santa Barbara St Pasadena, California 91101
[2] Theoretical Astrophysics, California Institute of Technology, Pasadena, CA 91125, USA

In Nissanke et al. 2013 (hereafter, Paper I), we undertook an extensive end-to-end simulation on how to identify the elusive EM counterpart of a GW detection of NS mergers. We started with simulated astrophysical populations of NS mergers, evaluated GW detectability and considered three critical steps: (1) GW sky localization and distance measures using different worldwide networks of three to five GW interferometers, (2) subsequent EM detectability by a slew of multiwavelength telescopes, and (3) identification of the merger counterpart amongst a possible fog of astrophysical false-positive signatures. We showed how constructing GW volumes and local Universe galaxy catalogs, can help identify and reduce the number of false-positives, thereby enabling a secure EM identification.

Paper I simulated mergers detected by a network of three to five GW interferometers. However, given projected timescales for construction of advanced GW interferometers, it appears that the early years (and possibly the first detections) could be limited to a network of only two LIGO interferometers (LIGO Scientific Collaboration 2013).

In this letter, we consider new observational challenges specific to a network of only two GW interferometers. We derive GW localization arcs (§2,§3), simulate detectability of EM counterparts (§4), discuss false positives (§5) and conclude with strategies for timely EM-GW identification of NS mergers (§6).

2. GW METHOD: DETECTION AND SOURCE CHARACTERIZATION

As detailed in §2 of Paper I, we construct an astrophysically-motivated population of 4×10^4 NS-NS binaries out to a limiting redshift $z = 0.5$. Parameters include: binary masses, luminosity distance D_L, inclina-

tion angle to the observer's line-of-sight $\cos\iota$, GW polarization angle ψ, and sky position $\mathbf{n}$ (where $\hat{\mathbf{n}} \equiv (\theta, \phi)$ is the unit vector pointing to a binary on the sky from a fixed Earth coordinate system, θ is the colatitude and ϕ is the longitude). We associate each binary with a random orientation and sky position, and distribute the mergers assuming a constant comoving volume density for $D_L > 200$ Mpc (ΛCDM, Komatsu et al. 2009) or using a B-band luminosity galaxy catalog (CLU; Kasliwal 2011) for $D_L < 200$ Mpc.

Next, we select the NS mergers that are detectable with only the two LIGO interferometers at positions $\mathbf{x_H}$ and $\mathbf{x_L}$ (the subscripts denote the Hanford and Livingston sites, hereafter LIGO-H and LIGO-L). GW detection and source characterization methods use optimum matched filtering between GW predictions and simulated detector streams (see §3 of Paper I for details). The measured GW strain h_M at a particular detector $\mathbf{x_H}$ or $\mathbf{x_L}$ is the sum of the two GW polarizations, h_+ and $h_\times$, each weighted by their antenna response functions $F_{+,[\mathbf{H/L}]}$ and $F_{\times,[\mathbf{H/L}]}$, and multiplied by a time-of-flight correction. The time delay of the signal between the detector and the coordinate origin is given by $\tau_{[\mathbf{H/L}]} \sim \hat{\mathbf{n}} \cdot \mathbf{x}_{[\mathbf{H/L}]}/c$, where c is the speed of light. h_+ and $h_\times$ are functions of D_L, $\cos\iota$, masses, and the GW frequency f. The antenna responses, $F_{+,[\mathbf{H/L}]}$ and $F_{\times,[\mathbf{H/L}]}$, depend on $\hat{\mathbf{n}}$ and ψ. Based on triangulation with three or more interferometers, the time delay factor dominates over amplitude effects in the GW waveform when reconstructing sky location errors for the majority of sources (Nissanke et al. 2011; Veitch et al. 2012).

For LIGO-H and LIGO-L, we assume two anticipated noise curves at mid and full sensitivity (the upper red and black lines in Figure 1 of LIGO Scientific Collaboration 2013) and idealized noise. We define a binary to be GW detectable if its expected signal-to-noise ratio (SNR) at each detector is > 6.5 and its expected network SNR (the root-sum-square of the individual SNRs) > 12. Consistent with §2.4 of Paper I, the term *Net2a* denotes a LIGO-H and LIGO-L network using such a coincident trigger, whereas *Net2b* corresponds to an expected network SNR trigger of > 8.5.

To infer the binary's sky position, we explicitly map out the full nine dimensional posterior probability density function (PDF) using MCMC methods (see §3 of Paper I and Nissanke et al. 2010) and derive 2-D PDFs in $(\cos\theta, \phi)$. We took particular care to start each MCMC chain at random all-sky positions.

Finally, to better understand our MCMC derived measures, we also implement two toy models using amplitude-only GW waveforms. The first model incorporates only time-of-arrival information, whereas the second incorporates a combination of time-of-arrival and the detector antenna responses. Our second toy model assumes a 5-D GW waveform of the form: $h_{T+F} \sim \exp^{i2\pi\tau f}\left[F_+(\hat{\mathbf{n}},\psi)\frac{(1+\cos^2\iota)}{D_L} + F_\times(\hat{\mathbf{n}},\psi)\frac{-2\cos\iota}{D_L}\right]$, where we take $f = 100$Hz. By simulating hundreds of noise realizations, we map out the likelihood function for $(\cos\theta, \phi)$ for randomly orientated and located binaries on the sky at different $\mathrm{SNRs}_{[\mathbf{H/L}]}$.

3. GW RESULTS: DISTANCE, LOCALIZATION ARCS, AND SKY SENSITIVITY

In Figure 1(a), we show the cumulative distance distributions of NS mergers detectable using only LIGO-H and LIGO-L at full-sensitivity. As expected, the distance distribution of mergers detected by Net2a is similar to those detected with Net3a-Net5a in §2 of Paper I. At mid-sensitivity, the distance distribution is scaled down by a factor of ~ 0.6.

In Figure 1(b), we show the cumulative histogram of sky localizations at 95% confidence regions (c.r.) for Net2a and compare the distribution with that estimated by Net3a–Net5a (§2 of Paper I). The median localization is 250 deg^2 compared with 17 deg^2 in Net3a. As in Paper I, we expect NS black-hole (BH) binaries to show a distribution similar to NS-NS. At mid-sensitivity, we expect the specific distribution in sky localizations to be similar to those at full-sensitivity because the majority of mergers will be detected at the SNR threshold (distribution not shown here due to small number of detections).

In Figure 2, we show the localization shapes, orientation and sky position of detected mergers at full-sensitivity. Using only time-of-arrival of signals at LIGO-H and LIGO-L, sky localization estimates have so far predicted annular error rings for non-spinning mergers of several thousand deg^2 (LIGO Scientific Collaboration 2013). Instead, we find that inclusion of $F_+(\hat{\mathbf{n}},\psi)$ and $F_\times(\hat{\mathbf{n}},\psi)$ in the GW waveform's amplitude significantly improves localization errors to arcs comprising several hundred deg^2. For Net 3–Net 5, we found that degeneracies between parameters result in non-contiguous areas for a handful of threshold mergers. (Nissanke et al. 2011). Furthermore, we do not measure mirror-image arcs on the sky for any of the detected binaries in our small sample. Indeed, for a single spinning NS-BH merger using two initial LIGO sensitivities, Raymond et al. (2009) generated a localization arc by including the BH's spin.

Investigations with our two toy models improve our understanding of the MCMC results. Using only time-of-arrival, averaging over a hundred noise realizations, we find GW localizations of almost annular rings of 1000s deg^2. Adding detector antennae information to the same binary, we find smaller GW arcs of 100s deg^2 in only one sky quadrant as long as the network SNR $>$ $\mathrm{SNR_{crit}}$, where $\mathrm{SNR_{crit}}$ ranges from 8–12 depending on orientation and sky position. Below $\mathrm{SNR_{crit}}$, the shapes depend on individual noise realizations and we find mirror images of GW arcs in different sky quadrants using h_{T+F}.

The quadrupolar antenna patterns of LIGO-H and LIGO-L are oriented such that they are sensitive to identical GW polarizations. Figure 2 shows that Net2 have significantly reduced sensitivity in two out of four sky quadrants for sources arriving in the plane of the interferometer arms. In contrast to Net3-5, we do not find a strong correlation between the D_L and sky error as a result of the two-quadrant sky sensitivity. We find that two binaries at the same distance can have localization areas differing by an order of magnitude based on sky position.

Out of our underlying population, we find that only 17±4 and 62±8 mergers are detected in GWs using Net2a and Net2b respectively. For the same population, we found that 43±7 and 144±12 mergers were detected us-

ing the corresponding Net3a and Net3b respectively (Table 1 of Paper I). Therefore, Net2 will detect $\approx$ 60% fewer mergers than Net3 using either SNR threshold. Using NS merger rate estimates (Abadie et al. 2010) and Eqn. (7) in Paper I, we expect 0.3–490 and 1.3–1640 mergers annually for Net2a and Net2b respectively.

4. EM DETECTABILITY (TRIGGERED): RESPONSE-TIME, TILING AND DEPTH

Our GW results, indicating a sky quadrant bias and coarse arc-shaped localizations, present new challenges for triggered EM follow-up. (The challenge for contemporaneous, independent detection in the γ-rays or X-rays or low frequency radio is unchanged.) Given the median localization of 250 deg^2 (at 95% c.r.), we find the tiling is currently beyond the scope of existing infrared, ultraviolet and millimeter facilities. Hence, we consider follow-up by a representative set of optical facilities, with telescope apertures spanning 0.5–8 m and camera angles spanning 2–50 deg^2 (see Table 1), and simulate relative detectability.

Due to the Net2 sky quadrant bias (Figure 2), mergers are preferentially detected overhead in the north and at hour angles around twelve in the south (relative to LST at LIGO-H/LIGO-L). Consequently, an EM observatory located around the same longitude as LIGO can respond instantly if located in North America but only half a day later in Chile (see Table 1). This time-lag in response is critical for afterglows, which fade as a power-law in time, and some kilonova models, which fade on few hours to day timescales. It is not relevant for radio facilities looking for late-time emission on the months to year timescale.

Due to the elongated arc-shape and the coarser localization of hundreds of deg^2, tiling presents a major challenge. We compute an optimal tiling pattern to cover the GW localization contour (95% c.r.) for each merger at each EM facility (Figure 3). While the widest cameras need < 20 pointings, other facilities need hundreds of pointings. Naive division of the localization area by the camera field of view grossly underestimates the actual number of pointings required. This tiling inefficiency factor has a median value of 1.6 for BG4/HSC, 1.8 for DECAM, 2.0 for LSST/PS1, 2.3 for ATLAS and 2.6 for ZTF. The localization arcs have a median width of 6.5° (in agreement with time-of-arrival estimates e.g., Fairhurst 2010). Narrow-angle cameras can tile more nimbly than wide-angle cameras (e.g., the BG4 tiling is 30% more efficient than the contiguous PS1).

With the number of pointings in-hand for each binary and for each EM facility, we compute the maximum exposure time (and hence, depth) allowable in a fixed duration. We assume three epochs (dithered to cover chip gaps) of one hour each with a detection above 5σ in at least two epochs as minimum criterion for EM detection. We take into account overhead between exposures which is dominated by readout for large mosaic cameras. Given the distance to each binary in our simulation, we convert the apparent magnitude depth to a luminosity.

Our detectability simulation results for Net2 are very different from those in Paper I for Net3–5. Figure 4 shows that small telescopes with large camera angles (e.g., ZTF) are *more* competitive than large telescopes with small camera angles (e.g., HSC) for detecting counterparts with an i-band luminosity brighter than $M_i = -14.5$ mag. Recent tantalizing near-infrared excess observed in one short GRB suggests bright kilonovae may be plausible (e.g., Tanvir et al. 2013). Note that response-time is not folded into this figure as there is a diversity in kilonova models ranging from some that rise by 1 mag and others that decline by 1 mag in the first 12 hours (Barnes & Kasen 2013).

Finally, EM follow-up is further hampered by weather, sunshine, lunation and visibility window. Thus, as discussed in §5.3 of Paper I, we emphasize that all detectable fractions presented here should be interpreted as relative.

5. EM IDENTIFICATION: FALSE POSITIVES

Optical detection of candidate EM counterparts in a single epoch is only the first step. Multiple epochs are essential to distill the true EM counterpart from thousands of astrophysical false positives in the foreground (e.g., moving objects in solar system, variable stars in Milky Way) and background (e.g., supernovae and AGN in higher redshift galaxies). An ongoing survey of the same sky location to a similar depth would provide a historic baseline of variability of unrelated sources and serve as a severe filter.

Timely identification of the EM counterpart is critical for obtaining spectroscopic and multi-wavelength follow-up before the transient fades. In §6 of Paper I, we considered five illustrative case studies to quantify the false positive challenge and solutions in various scenarios. Here, we revisit the same five binaries in the context of Net2.

A Beamed Merger (391 Mpc): On account of the sky quadrant bias, this merger is not detected by Net2 despite being beamed towards us. Given the lower rate of mergers detected with Net2 and the small fraction that is beamed (<2.5% for opening-jet angles $< 12°$), we may not have the luxury of the relatively easier search for the EM counterpart of a beamed merger in the early years of Net2.

A Close-in Merger (69 Mpc): Net2 localizes this merger to 23 deg^2 at full sensitivity and 32 deg^2 at mid-sensitivity. This is a factor of $\approx 40 - 50$ coarser than Net 3. Thus, the number of false positives would be proportionately larger and it is even more important to have a complete catalog of nearby galaxies. The fraction of "golden" binaries that are closer than 100 Mpc remains $\approx 10\%$.

A High Galactic Latitude Merger (139 Mpc): While Net 3 localized this merger to 19.5 deg^2, Net2 localizes this to 223 deg^2 at full sensitivity (it is not detected at mid-sensitivity due to its distance). Therefore, there are ten times more background sources and it is even more important to have a complete catalog of nearby galaxies and AGN variability.

A Low Galactic Latitude Merger (125 Mpc): While Net 3 localized this merger to 1.8 deg^2, Net2 localizes this to 100 deg^2 and 810 deg^2 at full and mid-sensitivity respectively. Thus, the foreground is 55 times larger and it is even more important to build a catalog of stellar sources.

A Galaxy Cluster Merger (115 Mpc):. On account of the sky quadrant location, this merger is not detected by Net2 despite being relatively nearby.

6. DISCUSSION

The EM-GW challenge for NS mergers is three-fold: the GW localizations are *wide* (few hundred deg^2) and the predicted EM counterparts are *faint* ($M_i \approx -12$ to -16 mag) and *fast* (few hours to few days). With LIGO-H and LIGO-L, we derive arc-shaped localizations with a median area of 250 deg^2 that are biased to only two sky quadrants. The rate of GW-detectable mergers is ≈40% of the rate of Net3 and the median localization area is 15 times coarser.

Strategies to maximize the odds of identifying faint and fast EM emission in wide GW arcs include:

- A network of small (< 1m) telescopes, despite the shallow depth, can leverage observatory location and wide-field to maximize rapid response to find bright and fast-evolving EM emission. Given the GW sky quadrant bias, North America and Southern Africa are recommended as the best locations for rapid response to Net2 triggers.

- A medium (1m–3m) telescope, despite the medium depth, can leverage an extremely large camera angle of few tens of deg^2 to be best positioned for searching for EM counterparts brighter than $M_i < -14.5$ mag. A dedicated facility with an ongoing survey to develop a baseline of historic variability is recommended.

- A large (> 4m) telescope, even with a relatively narrow camera angle of few deg^2, is uniquely positioned to find faint EM counterparts. A planned large time investment, facilitation of camera availability and minimization of overheads between pointings are recommended to be able to efficiently tile a larger fraction of mergers.

Independent of telescope size, the efficiency of a robust, real-time transient detection pipeline is an essential factor in assessing detectability. High quality image subtraction requires a deep pre-explosion reference image of the same sky location, preferably taken with the same EM facility. Reliable candidate vetting needs a veteran machine learning algorithm, preferably trained on a large set of previous transient detections by the same EM facility. Thus, two facilities with identical hardware but disparate software would have different EM-GW detection capabilities.

Ongoing surveys have already successfully demonstrated the capability to discover optical transients which overcome the challenges of wide/faint/fast, but one at a time. For example, the discovery of an afterglow in 71 deg^2 addresses the *wide* challenge (Singer et al. 2013), the discovery of multiple transients spanning kilonova luminosities addresses the *faint* characteristic (review in Kasliwal 2012) and the discovery of a relativistic explosion decaying on an hour timescale addresses the *fast* evolution (Cenko et al. 2013). Future surveys should prepare to simultaneously address all three challenges.

In summary, the early years of a small number of coarse GW localizations will be challenging but tractable for an EM search. The combination of camera angle, telescope aperture, observatory location and survey software for each EM facility will delineate a different range in EM emission timescale and luminosity. A multi-pronged EM search would provide robust constraints on the vast phase space of kilonovae (ejecta mass, velocity and composition). The findings of early searches will help plan EM-GW identifications to a larger number of better localized mergers in the era of three to five GW interferometers.

We thank C. Hirata and E. S. Phinney for careful reading of the manuscript. We acknowledge valuable discussions with E. Bellm, J. Bloom, Y. Chen, J. M. Désert, A. Georgieva, P. Groot, C. Galley, S. Mohta and D. Reitze. We thank D. Kasen for making kilonova models available. MMK acknowledges generous support from the Hubble Fellowship and Carnegie-Princeton Fellowship. SMN is supported by the David & Lucile Packard Foundation.

TABLE 1

Facility	Aperture (m)	Field-of-View (deg^2)	Exposure (sec)	Overhead (sec)	Sensitivity (5σ, i-mag)	Detectable Fraction (-16; -14; -12 mag)	Lag (hr)
Palomar: Zwicky Transient Facility (ZTF)[a]	1.2	47	600	15	22.2	0.94; 0.35; 0.06	1 ± 2
BlackGEM-4 (BG4)[b]	4×0.6	4×2	600	15	22.2	0.65; 0.12; 0.06	12 ± 2
Pan-STARRS1 (PS1)[c]	1.8	7.0	180	10	21.9	0.76; 0.18; 0.06	3 ± 2
ATLAS[d]	0.5	30	600	5	21.0	0.53; 0.06; 0.06	3 ± 2
CTIO: Dark Energy Camera (DECAM)[e]	4.0	3.0	10	30	22.8	0.53; 0.47; 0.12	12 ± 2
Subaru: HyperSuprimeCam (HSC)[f]	8.2	1.77	1	20	22.4	0.47; 0.47; 0.18	3 ± 2
Large Synoptic Survey Telescope (LSST)[g]	8.4	9.6	1	2	22.4	1.00; 1.00; 0.65	12 ± 2

[a] Kulkarni 2012, E. Bellm priv. comm.
[b] P. Groot priv. comm., BG plans up to 20 telescopes, see https://www.astro.ru.nl/wiki/research/blackgemarray
[c] http://pan-starrs.ifa.hawaii.edu
[d] J. Tonry priv. comm.
[e] D. DePoy priv. comm., Bernstein et al. 2012
[f] http://www.naoj.org/cgi-bin/img_etc.cgi
[g] LSST Science Collaborations 2009

REFERENCES

Aasi and LSC et al. 2013, arXiv: 1304.0670
Abadie, J., et al. 2010, Classical and Quantum Gravity, 27, 173001
Accadia, T., et al. 2011, Classical and Quantum Gravity, 28, 114002
Barish, B. C., & Weiss, R. 1999, Phys. Today, 52, 44
Barnes, J., & Kasen, D. 2013, arXiv:1303.5787
Bernstein, J. P., et al. 2012, ApJ, 753, 152
Cenko, S. B., et al. 2013, ApJ, 769, 130
Eichler, D., Livio, M., Piran, T., & Schramm, D. N. 1989, Nature, 340, 126
Fairhurst, S. 2011, Class. Quantum Grav., 28, 105021.
Grossman, D., Korobkin, O., Rosswog, S., & Piran, T. 2013, arXiv: 1307.2943
Hansen, B. M. S., & Lyutikov, M. 2001, MNRAS, 322, 695
Kasen, D., Badnell, N. R., & Barnes, J. 2013, arXiv: 1303.5788
Kasliwal, M. M. 2011, PhD thesis, California Institute of Technology
—. 2012, Publications of the Astronomical Society of the Pacific, 29, 482
—. 2013, Science, 340, 555
Komatsu, E., et al. 2009, ApJS, 180, 330
Kulkarni, S. R. 2005, arXiv: 0510256
—. 2012, arXiv: 1202.2738
Lattimer, J. M., & Schramm, D. N. 1976, ApJ, 210, 549
Lewis, A., & Bridle, S. 2002, Phys. Rev. D, 66, 103511
Li, L.-X., & Paczyński, B. 1998, ApJ, 507, L59
LSST Science Collaborations et al. 2009, ArXiv e-prints
Mathews, G. J., & Cowan, J. J. 1990, Nature, 345, 491
Metzger, B. D., et al. 2010, MNRAS, 406, 2650
Nakar, E., & Piran, T. 2011, Nature, 478, 82
Narayan, R., Paczynski, B., & Piran, T. 1992, ApJ, 395, L83
Nissanke, S., Holz, D. E., Hughes, S. A., Dalal, N., & Sievers, J. L. 2010, ApJ, 725, 496,
Nissanke, S., Kasliwal, M., & Georgieva, A. 2013, ApJ, 767, 124, referred to in the text as Paper I
Nissanke, S., Sievers, J., Dalal, N., & Holz, D. 2011, ApJ, 739, 99
Paczynski, B. 1991, Acta Astronomica, 41, 257
Piran, T., Nakar, E., & Rosswog, S. 2012, arXiv:1204.6242
Pshirkov, M. S., & Postnov, K. A. 2010, Ap&SS, 330, 13
Raymond, V., van der Sluys, M. V., Mandel, I., Kalogera, V., Röver, C., & Christensen, N. 2009, Classical and Quantum Gravity, 26, 114007
Roberts, L. F., Kasen, D., Lee, W. H., & Ramirez-Ruiz, E. 2011, ApJ, 736, L21
Rosswog, S. 2013, Royal Society of London Philosophical Transactions Series A, 371, 20272
Sigg, D., & the LIGO Scientific Collaboration. 2008, Classical and Quantum Gravity, 25, 114041
Singer, L. P., et al. 2013, arXiv: 1307.5851
Somiya, K. 2012, Classical and Quantum Gravity, 29, 124007
Tanaka, M., & Hotokezaka, K. 2013, arXiv:1306.3742
Tanvir, N. R., Levan, A. J., Fruchter, A. S., et al. 2013, Nature, in press, arXiv:1306.4971
van der Sluys, M., Raymond, V., Mandel, I., Röver, C., Christensen, N., Kalogera, V., Meyer, R., & Vecchio, A. 2008, Classical and Quantum Gravity, 25, 184011
Veitch, J., et al. 2012, Phys. Rev. D, 85, 104045

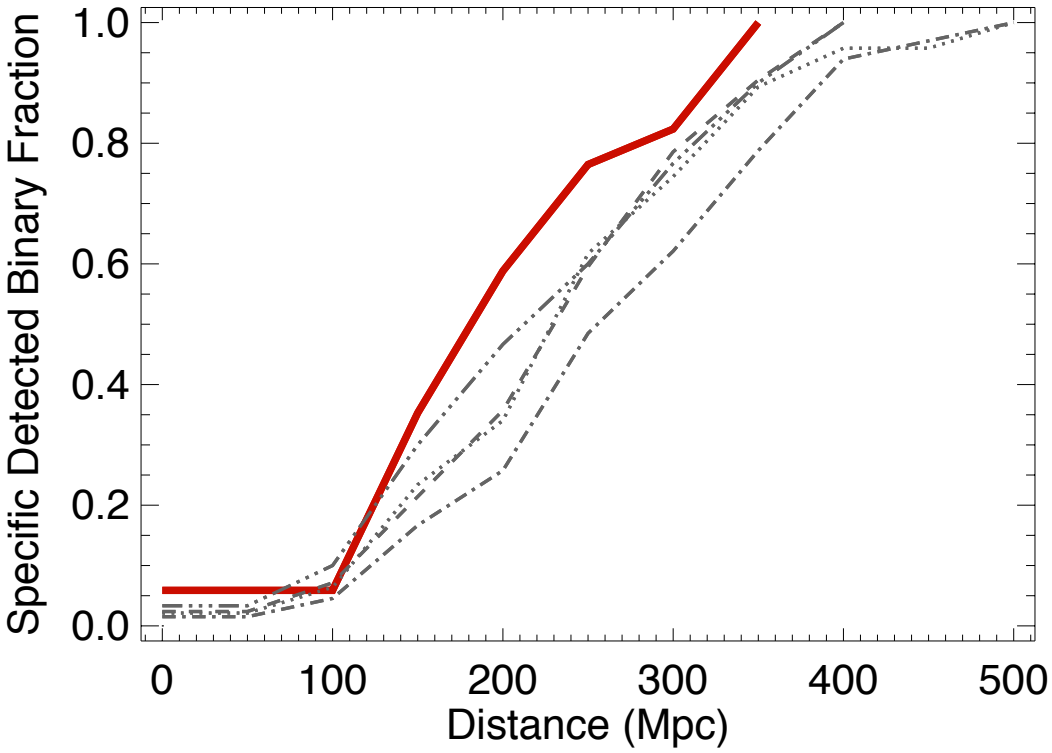

(a) NS-NS mergers: Luminosity Distance

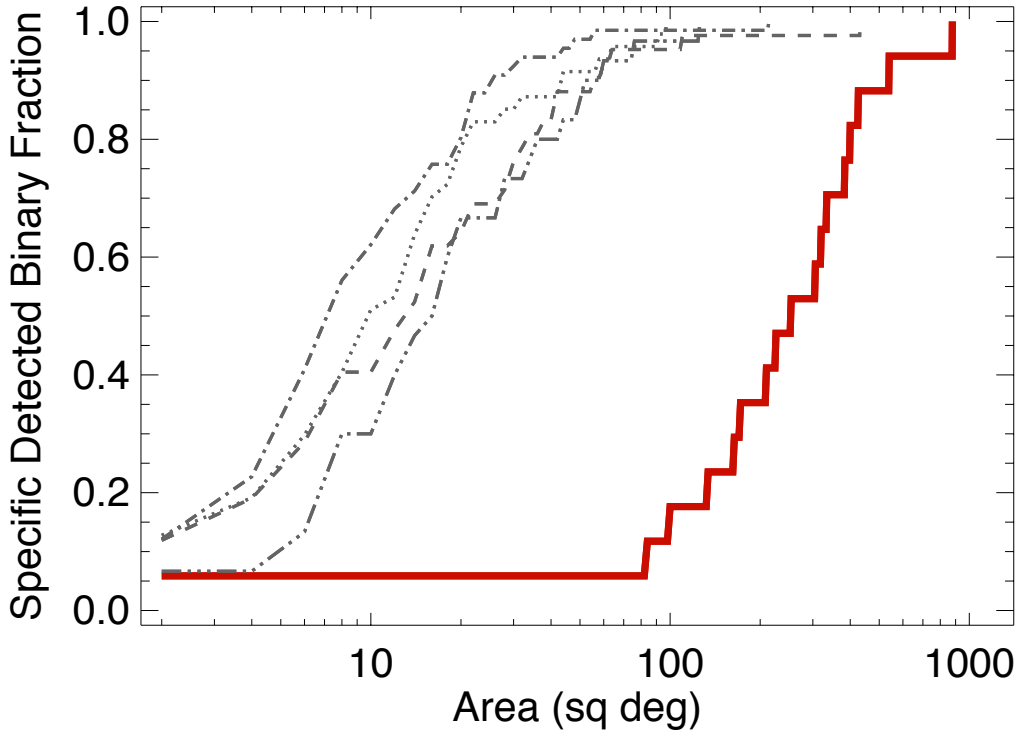

(b) NS-NS mergers: Sky errors

FIG. 1.— Cumulative distribution in luminosity distance (top panel) and 95% confidence sky error (bottom panel) of NS-NS mergers. Red lines denote a network of two GW interferometers. Gray lines denote Net 3–5 as presented in Paper I. We require an expected network SNR>12 and normalize to each specific network.

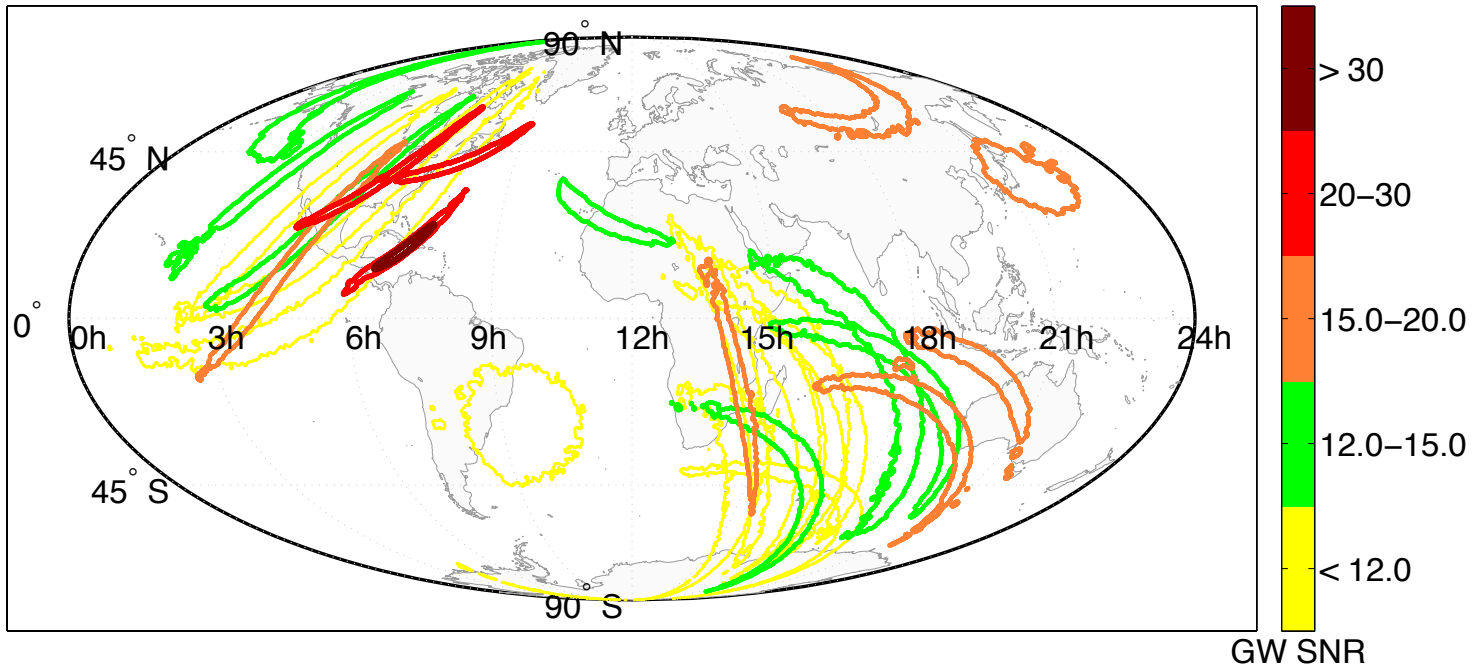

FIG. 2.— Sky location and localization arcs of mergers detected by LIGO-H and LIGO-L. Color represents expected network SNR. Note that the quadrupolar antenna pattern has a bias towards two sky quadrants. The rate of detected mergers is ≈40% of the rate of a three interferometer network. The EM observatory location dictates a time lag in response to GW trigger of up to to one day (Table 1).

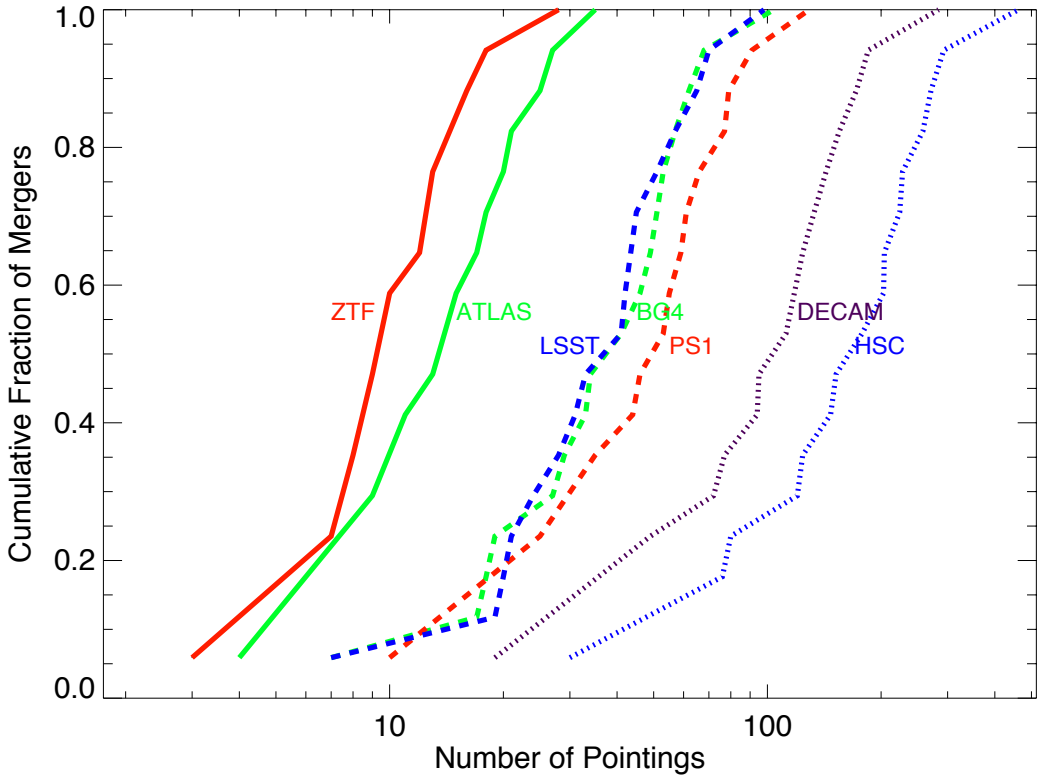

FIG. 3.— Cumulative distribution of number of pointings necessary to tile localization arcs at all sky positions by LIGO-H and LIGO-L. Color represents telescope diameter: 0.5m-class (green), 1m-class (red), 4m-class (purple) and 8m-class (blue). Line style represents camera angle: few tens of deg^2 (solid), several deg^2 (dashed) and few deg^2 (dotted).

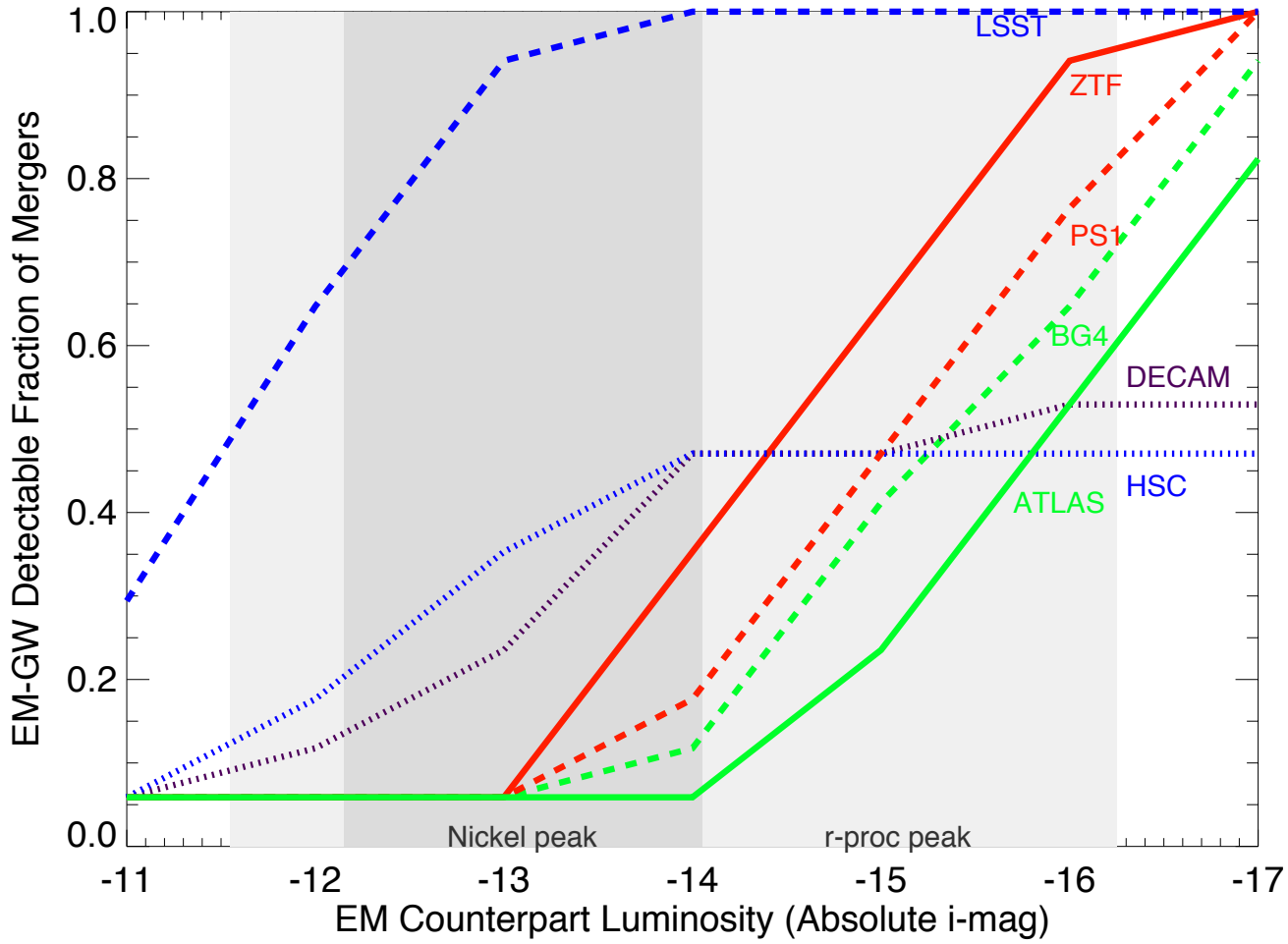

FIG. 4.— Fraction of mergers detectable by a given EM facility as a function of kilonova luminosity (expressed in absolute i-band AB magnitude). Color and line-styles are same as in Figure 3. Shaded regions denote theoretical predictions for kilonovae (Barnes & Kasen 2013; Kasen et al. 2013) — r-process powered peak (light grey; $M_{ejecta} \approx 10^{-1}$–$10^{-3}$ $M_{\odot}$, $v_{ejecta} \approx$ 0.1c–0.3c) and Nickel-56 powered peak (dark grey; $M_{ejecta} \approx 10^{-2}$–$10^{-3}$ $M_{\odot}$). All fractions are relative as an accessibility window of three hours with clear weather is assumed for all binaries at all facilities and no correction is made for lag in response (Table 1).